JOURNAL OF PETROLEUM GEOMECHANICS
(JPG)

Multiscale Multiphysic Mixed Geomechanical Model for Deformable Porous Media Considering the Effects of Surrounding Area

Hasan Ghasemzadeh
Associate Professor; Faculty of Civil Eng., K. N. Toosi University of Technology, ghasemzadeh@kntu.ac.ir

Received: 19 Dec 2019; Accepted: 22 Feb 2019

DOI: 10.22107/JPG.2019.88412

Keywords

Geomechanics
Deformable storages
Elasto-plastic
Multiscale
Adaptive mesh refinement
Deformable environment

Abstract

Porous media of hydro-carbon reservoirs is influenced from several scales. Effective scales of fluid phases and solid phase are different. To reduce calculations in simulating porous hydro-carbon reservoirs, each physical phenomenon should be assisted in the range of its effective scale. The simulating with fine scale in a multiple physics hydro-carbon media exceeds the current computational capabilities. So, the Improved Multiscale Multiphysic Mixed Geomechanical Model (IM^3GM), has been recently developed. An elaso-plastic model which consider the hydraulic and mechanical behaviors of media is used to simulate the solid phase deformation in IM^3GM. Also, the multiscale and adaptive mesh refinement (AMR) method is used to reduce the computational time. In this study, IM^3GM is introduced by simulating the effects of surrounding area of reservoirs. Finally, a reservoir sample is simulated by IM^3GM and reasonable agreements are obtained. It seems that the effect of surrounding area is undeniable and should be taken into consideration.

1. Introduction

The behavior of hydro-carbon reservoirs in the past and future is studied by numerical modeling. To determine the optimal location for injection and production wells of these reservoirs, lots of simulations have been done. Also, it should be kept in mind that simulating fluid flow in porous media is only one step of the many sections for optimal production of the oil reservoirs. It is needed to more accurate results and less time duration to better behavior prediction and managements of reservoirs. So, decreasing the number and duration of calculations will be necessary and greatly welcomed. Several natural porous media, especially hydro-carbon reservoirs, have severe heterogeneities in a wide area of scales. These heterogeneities show themselves in form of intense changes in permeability field. Therefore, the flow of liquid inside porous media is a multi-scale phenomenon.

Generally, a natural porous medium (like a hydro-carbon reservoir) is of heterogeneous structure such as discrete crack, impermeable cavities and layers. As a result of these heterogeneities, some qualities of porous medium such as porosity and permeability have random structure, and intensively change during time. In fact, the value of

permeability can change discretely in an area, to some large-scale. Flow of liquid inside porous media is generally considered to be a multiscale phenomenon. The main reason for multiscale behavior of flow of liquid in an oil (hydro-carbon) reservoir is heterogeneity in the reservoir rock, which are from the size of cavities (from micron to millimeter) to scales of the same size as the oil reservoirs (about kilometers). On the other hand, heterogeneities with very small scales have great effects on the behavior of liquid flow in larger scales [1]. This fact has led to production and development of geological models for describing and estimating the characteristics of oil reservoirs with high separation degrees. Using these models, the permeability changes method (porosity) of the reservoir will be available with high separation degree. In this study, the permeability field with high separation degree is called micro-scale data.

Geological models of the micro-scale data of permeability field (also porosity) of a reservoir is expressed with a network containing $10^6 – 10^9$ cells (freedom degree); that is while current industrial simulations are able to compute models with $10^4 – 10^6$ freedom degree (computational cell). Therefore, there is a distance between the level of details in describing oil reservoirs and the ability of industrial simulations [3]. This vast distance between the levels of data causes that micro-scale (using all details) simulation of liquid flow in an oil reservoir would not be possible. Since the volume of input data is high, simulating such flows requires using computers with very high memory volume and running time, which is very costly and even impossible in some cases. It is necessary to consider the effect of all the heterogeneities of the reservoir rock in order to achieve accurate predictions of the behavior of liquid inside an oil reservoir. In recent years, multiscale methods have been applied, as an imperial tool to solve this problem. A phenomenon which consists of a series of physical processes within a wide range of time and scales is called a multiscale phenomenon. Many of the practical problems have multiscale behavior. Heat transfer in compound material, flow of liquids inside porous media and turbulent flow are examples of these problems [2].

In multiscale method each physical phenomenon is implemented within the area of its efficiency. So, the number of calculations is considerably decreased without any decrease in accuracy. It is usual to use the multiscale finite volume method for fluid phases in interaction with the finite elements method for solid phase. Due to mass conservation in the multiscale finite volume (MsFV) method, this method is appropriate for modelling the fluid phases of porous oil reservoirs. MsFV method produces an unconventional pressure field. A series of local problems are defined and solved in each binary block when the dual network is specified. The result of each of these local problems is called a basic function. It should be noted that the values of local microscale permeability (inside each dual block) should be used for computing each of these basic functions. Using basic functions, a macroscale transferability is computed, and then a macroscale system is established. The microscale pressure field is formed using from basic functions and macroscale pressure distribution. In other words, microscale pressure is written in form of the linear combination of macroscale pressure field. This method has been instituted since 2003 by Jenny et al. [4]. At first, this model was

presented in a two dimensional mode for one phase and by disregarding capillary and solubility. In this equation method, mass is partitioned into two equations, pressure equation and saturation degree equation. First, pressure equation is satisfied on the coarse meshing. Then, considering mass conservation, the equation of saturation degree satisfies upon solving permanent pressures on fine meshing. The model presented was upgraded to a two phase mode by Jenny et al. in 2004 [5].

After this, in 2006, Lunati and Jenni [1] defined another series of local problems for considering side effects such as the existence of well and gravity effects in MsFV method. In the framework of MsFV methods, the reply to each series of these local problems is called corrective functions. It should be mentioned that basic and correction functions are respectively expressive of general response and private response of the problems define inside dual blocks. MsFV method has been expanded to multiphase flows by different scientists such as Jenni, Tchelepi, Lunati and Lee, considering the effect of compressibility (reservoir rock and fluid), capillary pressure and gravity [6-9]. This was expressed in the multiscale finite volume method, based on operational (matrix) formulization, by Zhou and Tchelepi in [10] and also by Lunati et al. in [11]. A new series of MsFV methods, named iterative multiscale finite volume method *(*i- MsFV*)* was introduced by Hajibeigi et al. in 2008 and 2009 [12, 13] in which the responses of multiscale method converged to a microscale response during iterative operations. Although for a wide range of problems, iterative process in microscale finite volume leads to the convergence to microscale solving [14], in some problems, even by exerting iterative process, the answer could not be converged to microscale solving. Considering the geological effects of the source rock and its surrounding area, and using the multiscale finite volume method has been done by Taheri [15, 16]. Also recently, measures have been taken to improve the accuracy of the model by using a combine problem solving method for problems with central and local coordinates [17].

It should be noted that some of the oil reservoirs are deformable, several damages due to displacements can influence on instability of the equipments where are located on the top of these reservoirs and also environmental damages. On the other hand, solid phase displacements not only damaged the upper hand equipment, but also caused a change in the flow direction. Reservoir deformations occur due to the changes in cavity pressure of the effective tensions, which are affect the reservoir production. It is requires that geomechanical and flow equations to be solved, simultaneously. Since these two phenomena are mutually interacted, considering deformation effects in reservoir simulation. On the other hand, assessing the mechanical behavior of the porous media, has a great importance in simulation of oil reservoirs. For example, geo-mechanical analyses in design of hydraulic failure systems, well stability analysis and analysis of extraction systems inside deformable storages could be pointed out. In this type of reservoirs, deformations of the reservoir rock are considered as an effective phenomenon in production value. These deformations occur due to variation of cavity pressures and hence the effective stress changes in the reservoir rock. Two key parameters are involved in determining the

flow inside reservoir, porosity value and permeability. Generally, extracting oil from a reservoir in long term results in the cavity pressure reduction. This decrease leads to increase the effective stress in reservoir layers and decrease the reservoir volume. On the other hand, the cavity fluid pressure inside the reservoir increases by injection during the secondary extraction. So, a reduction in the effective stress and hence inflation of the reservoir will be observed. The solid deformations can affect the efficiency of the reservoir due to affecting porosity and rock permeability value and also by making changes in reservoir pressure. Considering the reservoir depth and different stratifications of the ground, reservoir deformations may not have a significant impact on the surface of earth. However, in some cases (such as Wilmington field) even a settlement of 9 meters has been reported [18].

Constitutive models for unsaturated soils and rocks which consist of coupling hydraulic and mechanical behaviors are interesting subjects in geotechnical studies. The influence of saturation degree and volumetric strain on mechanical and hydraulic behavior are considered in constitutive models, respectively. Net stress and matric suction (pore air pressure minus pore water pressure) or effective stress and modified matric suction have been widely used as two stress-state variables in order to survey the hydro-mechanical behavior of soils [19-21]. Muraleetharan et al. found that intergranular stress tensor and matric suction are appropriate stress state variables for considering the behavior of water volume fraction on the stress and strain of the soil [22]. The mentioned models are capable of simulating hydraulic behaviors such as multiple cycles of wetting and drying. But, they cannot capable for mechanical loading and unloading simulation. Also, the motion of the mean wetting and drying curves is not coupled with plastic deformation. Ghasemzadeh proposed an elastoplastic model for unsaturated deformable porous media [23]. Recently, several researchers proposed elastoplastic constitutive models in which the deformation influences on soil-water characteristic curves and coupling effects are considered [24-26]. A coupled hydro-mechanical model was introduced for unsaturated soils by Ghasemzadeh and Ghoreishian Amiri using from intergranular stress and matric suction as stress-state variables under just isotropic loadings [27]. In this model, the constitutive equations and coupled hardening rules were added to Muraleetharan et al. model. So, this model is qualified for considering the effects of mechanical loading or unloading on water volume fraction. Ghasemzadeh and Ghoreishian Amiri's model was developed by Ghasemzadeh et al. [28] to cover anisotropic loading conditions. In this model, plastic deformation and capillary hysteresis of unsaturated soils are considered. This model was developed by Ghasemzadeh and Sanayepasand [29] for general stress state loading conditions. Also, the oil phase was added to this model. Finally, this model was calibrated for unsaturated porous media.

The assumption of considering multiscale coarse networks (separation degree) seems to be useful for solid phase. This is performed by adding adaptive mesh refinement (AMR) to coarse network of this phase. This method can cover the simulation problems of heterogeneous reservoirs by utilizing more accuracy only in the domains which require that. This method is applicable

to temporally varying resolution. AMR may be accomplished at every time-steps of simulation if it be needful to improve the efficiency and accuracy. This method can re-mesh the areas containing high density of heterogeneity and entrance data. An interpolation is used to determine the quantities of momentum and volume fraction in the refined network [30]. AMR method consists of two categories, structured and unstructured, for refining the mesh network. The types of coarse and revised networks are the same in the structured classification. But, these are different in the unstructured one. So, the refinement ratio is constant in the structured classification at each level of refinement. Mesh refinement should be done in such a way that all of the grids in the previous network are used in the modified one. Regular bisection method is one of the ways to subdivide the elements in structured category. In this method a grid is added at the middle of the sides of the element and the element is divided to four refined elements. So, the refinement ratio is two. In AMR method, the error function is calculated in every mesh after an iteration. Mesh network is refined in the areas where the calculated error is more than the allowed error rate.

The grids and grids data of each level are used in the next level of refined meshes [31, 32]. The main problem in this method is in the interface between coarse and fine meshes [33]. Specific attention should be performed at the contact points of refined meshes with the adjacent previous meshes, in order to maintain consistency and convergence of the model [34-36]. AMR method was used on solid phase coarse cells of IM^{3}GM by Ghasemzadeh and Sanayepasand [29, 37] to increase the accuracy in some zones of storages after adding the elastoplastic model. The reservoir system must be completely modeled with its surrounding rocks, according to the fact that reservoir deformation is also affected by the rigidity of its surrounding environment. The effect of surrounding boundary conditions on the reservoir mechanical behavior is totally ignored in the models.

An unreal boundary condition can cause to model reservoir deformations and hence the distribution of effective stress and fluids pressure, totally away from reality. Rothenburg in 1994 [38], pointed out the importance of modeling a reservoir surrounding environment in the accuracy of the model answers. But, considering wide area of surrounding environment can cause to increases the computation cost to a great extent due to the number of elements and the number of freedom degree inside each element. However, some of the researchers have taken an action toward this type of modeling and have shown its importance [39-41]. Considering the effect of reservoir surrounding environment on their deformations, it is necessary to add the surrounding rocks to a model. But, modeling the vast area of surrounding rocks can increase the number of elements, unknowns and the cost of simulation. So, the surrounding effects has been considered only on reservoirs borderlines [42-44].

The aim of this study is to introduce IM^{3}GM, considering the effects of surrounding rock on solid phase deformation. In the following of this article, the governing equations, the utilized elastoplastic model, the utilized AMR method, the considered surrounding strata with virtual springs and numerical model are presented, respectively. Finally, to assess accuracy and efficiency of

the proposed method, the indicative test cases is analyzed.

2. Governing equations

In this work, three nonlinear, compressible and irresolvable fluid flows consists of oil, water and gas with deformable solid skeletons are modeled considering capillary effects between fluid phases. The equations are parabolic due to compressibility and capillary (rock and fluid). In most of the problems, convection prevails the process of reservoir displacement. As a result, pressure field is usually elliptical, and saturation equations often have hyperbolic behavior. General calculation of pressure is categorized to two elliptical parts, floating-dominant and capillary-dominant. Impact of wells on flow is shown in private solutions of these equations. The principle multiscale algorithm of finite volumes was designed for computing the pressure of incompressible flows (elliptical) in very heterogeneous forms. The current model, which is applied considering capillary, makes a parabolic nonlinear pressure equation. However, these effects are generally of local nature, and pressure equation usually shows a behavior close to elliptical behavior.

The assumptions which the model equations are based on them are: 1.The solid particle is incompressible. 2. The behavior of the solid skeleton is elasto-plastic.3. The deformations and their gradients are assumed to be so small. 4. Fluid flow obeys Darcy's law. 5. There is no mass exchange among the phases. 6. Capillary effect is considered in fluid phases. 7. The effects of temperature are ignored. 8. Fluid flow and solid phase deformation are modelled by different structures and under unequal criteria. So, we have a nonlinear parabolic pressure equation. The governing equation in deformable porous medium consist of mass conservation and momentum conservation equations in fluid phases and solid phase, and in structural equations. Substituting the momentum balance of fluid and solid equations in mass balance equation of fluid, we have the following equation. Substituting the momentum conservation relations of fluid phases and also the relations of the mass conservation and momentum conservation of the solid phase in the mass conservation relation of fluid phase, the following relation for each phase is obtained. For more details, please refer to [15].

$$\phi \frac{D^S}{Dt} S_\alpha \rho_\alpha + S_\alpha \rho_\alpha \frac{D^S \phi}{Dt} + \nabla . \left(\rho_\alpha \frac{K k r_\alpha}{\mu_\alpha} . \left[-\nabla p_\alpha + \rho_\alpha g \right] \right) + \phi S_\alpha \rho_\alpha \frac{\varepsilon_{VOL}}{\Delta t} = \dot{m}_\alpha \qquad (1)$$

In the above relation, ϕ is porosity, ρ_α is specific gravity of a phase, S_α is saturation degree of a phase, K is the absolute permeability tensor, k_{ra} is relative permeability, μ_α is the phase viscosity and $\dot{m}_\alpha$ denotes sink and source terms. Given that the number of unknowns is more than the number of equations in the governing equations, we have some conservation equations such as the continuity of degree of saturation, porosity and density, the equation between permeability and degree of saturation, the relationship between density and pressure and also, the difference between pressure of fluid phases r for considering capillary pressures. The implicit discretization of eq.

(1) with considering the capillary pressure, leads to:

$$\varphi^{n+1}\frac{\rho_\alpha^{n+1}.S_\alpha^{n+1}-\rho_\alpha^{n}.S_\alpha^{n}}{\Delta t}+\rho_\alpha^{n}.S_\alpha^{n}.\frac{\varphi^{n+1}-\varphi^{n}}{\Delta t}-\nabla.\left(\rho_\alpha^{n+1}.\lambda_\alpha\left(\nabla\left(p+p_{c\alpha o}\right)^{n+1}-\rho_\alpha^{n+1}.g.\nabla z\right)\right) \quad (2)$$
$$+\left(\varphi^{n+1}.\rho_\alpha^{n+1}.S_\alpha^{n+1}\right).\frac{\varepsilon_v^{n+1}-\varepsilon_v^{n}}{\Delta t}=\rho_\alpha^{n+1}.q_\alpha$$

where $p_{c\alpha o}=p_\alpha-p_o$, q is a volumetric sink/source term, n and $n+1$ show two sequential time steps. The above equations have a combination of pressure and volume strain. First, these equations are solved in fluid phases and the pressure is obtained. Next, the deformation is obtained in solid phase based on the pressure. The cycle is iterated till converged by Newton Raphson's cycle. The above equations should be multiplied in α to obtain decoupled pressure. This value is calculated from $\alpha_a=1/\rho_a^{n+1}$ for different phases. Then, by taking the sum over all phases and linearization, the eq. (3) is obtained.

$$C\frac{\left(p^{v+1}-p^{v}\right)}{\Delta t}-\sum_{i=1}^{n_p}\alpha_i.\nabla.\left(\lambda_i^{nv}.\nabla p^{v+1}\right)=RHS \quad (3)$$

where $\lambda_O^{nv}=\rho_O^{v}.\lambda_O^{v}$, $\lambda_W^{nv}=\rho_W^{v}.\lambda_W^{v}$ and $\lambda_g^{nv}=\rho_g^{v}.\lambda_g^{v}$. Also, v and $v+1$ show the pressure in two sequential iterations. The compressibility index (C) and RHS are obtained from below equations.

$$C=\frac{\partial\phi}{\partial p}\bigg|^{v}-\phi^{n}\sum_{i=1}^{n_p}\frac{\partial\alpha_i}{\partial p}\bigg|^{v}\rho_i^{n}S_i^{n}+\Delta t\sum_{i=1}^{n_p}\frac{\partial\alpha_i q_i}{\partial p}\bigg|^{v} \quad (4)$$

$$RHS=-\frac{\phi^{v}}{\Delta t}+\frac{\phi^{n}}{\Delta t}\sum_{i=1}^{n_p}\alpha_i\rho_i^{n}S_i^{n}+\sum_{i=1}^{n_p}\alpha_i\rho_i^{v}q_i^{v}-\sum_{i=1}^{n_p}\alpha_i.\nabla.\left(g\rho_i\lambda_i^{nv}.\nabla z\right)$$
$$+\alpha_W.\nabla.\left(\lambda'_W.\nabla p_{CWO}\right)^{v}+\alpha_g.\nabla.\left(\lambda'_g.\nabla p_{CgO}\right)^{v}-\phi^{v}\frac{\varepsilon_v^{v}-\varepsilon_v^{n}}{\Delta t} \quad (5)$$

3. An elastoplastic model of IM^{3}GM for simulating the solid phase

In this section, the constitutive coupled hydro-mechanical elastoplastic model, which is utilized in IM^{3}GM, is described. This model is the improved of the model which was proposed by [27, 28]. The model improvement is classified to three parts. First, the model is calibrated for an unsaturated porous media. Next, the oil phase is added to the model, and the model equations are improved from isotropic and deviatoric loadings to general stress state loading. The model has efficient constitutive equations and hardening rules to simulate the unsaturated soils under cyclic isotropic and deviatoric loads. The two stress-state variables of the model are an

intergranular stress and a matric suction. The loading collapse (LC) yield surface is used in this model to consider the influences of widening and narrowing. Also, the suction increase (SI) and suction decrease (SD) yield surfaces are utilized for considering the plastic change of n_w in drying and wetting paths, respectively. The mentioned yield surfaces are shown in Fig. 1. Seven stress-strain parameters (F_0, k, K, m, λ_s, υ and u), nine hydraulic parameters (b_1, d_1, b_2, d_2, $n_{w_{res}}$, $n_{w_{sat}}$, h, g, and Γ^e) and two coupling parameters (α_1, α_2) are required in the model. These parameters and the values of these parameters for a clay sample and a porous media sample, which are obtained after calibration are described in Table 1. These parameters should be obtained for each porous media and added to IM^{3}GM as input parameters, before each simulation.

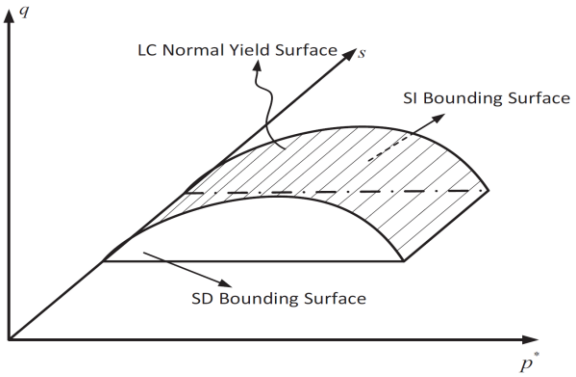

FIG 1. schematic of LC, SI and SD yield surfaces

TABLE 1. Parameters definition for the elastoplastic model and the calculated values for two samples

Parameter	Definition	Pearl clay	Porous media sample [45]
F_0	Pre-consolidation pressure	220 kPa	100 kPa
u	This calibration parameter which is found from soil stress-strain diagram.	150	200
k	The slopes of swelling lines in $\nu - \ln p^*$ plane	0.07	0.018
m	The slope of the critical state line	0.88	1.05
λ_s	The slope of the normal consolidation line in $\ln\nu - \ln p^*$ plane	0.045	0.05
K	The slopes of swelling lines in $\ln\nu - \ln p^*$ plane	0.009	0.0041
υ	Poisson's ratio	0.25	0.365
b_1	Material parameters which describe the primary wetting and secondary drying curves in the $s - n_w$ space. The value of this parameter can be determined by conducting curve-fitting procedure. b_1 and b_2 have the same value for porous media.	22 kPa	2.3 kPa
d_1		1.635	0.5
b_2		105 kPa	2.3 kPa
d_2		4.8	1.05
Γ^e	Capillary elastic modulus which is found from scanning curves.	-2330 kPa	-12.46 kPa
h	A model parameter which can be found from scanning curves.	10	7
g	A model parameter which typically ranges from 0.1 to 2.0. It is set to be 1.0 for porous media.	0.1	1
$n_{w_{sat}}$	The maximum value of n_w at the primary wetting curve	0.492	0.51
$n_{w_{res}}$	The minimum value of n_w at the secondary drying curve	0.305	0.21
α_1	Coupling parameter which can shift the value of $n_{w,sat}$ or $n_{w,res}$ due to any plastic deformation.	0.1	1
α_2		0.1	0.1

Considering the fact that there are two liquid phases of water and oil in oil reservoirs simultaneously, the liquid volume fraction (n_l) is used in the improved equations, instead of water volume fraction (n_w). The liquid volume fraction is defined in terms of water volume fraction and oil volume fraction (n_o), as below.

$$n_l = \frac{v_l}{v} = \frac{v_w + v_o}{v} = n_w + n_o \quad (6)$$

Mechanical and hydraulic behaviors are characterized by subloading and bounding surfaces, respectively. Coupling between these behaviors is done by hardening rules. Normal yield surface and bounding surface functions are as follows:

$$f(\sigma^*) = \frac{\sigma_x^* + 2\sigma_y^*}{3} + n_l.s.I + \frac{2(\sigma_x^* - \sigma_y^*)^2}{(\sigma_x^* + 2\sigma_y^*)m^2} = F(H) \quad (7)$$

$$F = F_0 \exp(\frac{H}{\lambda_S - K}) \quad (8)$$

$$s_{D0} = b_1[\frac{n_{l_{sat}} - n_l}{n_l - n_{l_{res}}}]^{\frac{1}{d_1}} \quad (9)$$

$$s_{I0} = b_2[\frac{n_{l_{sat}} - n_l}{n_l - n_{l_{res}}}]^{\frac{1}{d_2}} \quad (10)$$

where F is the position of the surface which is a function of the hardening variable (H). Also, s_{I0} and s_{D0} are the positions of SI and SD surfaces, respectively. Coupled hardening functions are:

$$dH = d\varepsilon_v^p - dn_l^p \quad (11)$$

Introducing both of LC normal yield and subloading surfaces is essential for having constitutive equations in the model. The subloading surface has a shape similar to the LC normal yield surface, which is placed inside the LC surface. The subloading surface usually passes from the current stress point. This surface is defined as follows:

$$f(\sigma^*) = R.F(H) \quad (12)$$

where R is the ratio of similarity between LC normal yield surface and subloading surface. FEM is used to simulate the solid phase of an oil reservoir. Using FEM in order to solve the equations of the mentioned elastoplastic model leads considering the compatibility requirement, as follows:

$$dF = \left(\frac{\partial f}{\partial \sigma}\right)^T \cdot d\sigma + \left(\frac{\partial f}{\partial H}\right)^T \cdot dH = 0 \quad (13)$$

The last equation is converted to Eq. (17), considering the below equations.

$$dn_l^p = \left(\frac{1}{\Gamma^e} + \frac{1}{\Gamma^p}\right).ds + \frac{N^T.N.n_l}{M^P}(d\sigma + n_l.ds + s.dn_l) = Y.d\sigma + W.ds \tag{14}$$

$$dH = d\varepsilon_v^p - dn_l^p = d\varepsilon_v^p - Y \cdot d\sigma - W \cdot ds \tag{15}$$

where $Y = \frac{N^T.N.n_l}{M^P - N^T.N.n_l.S}$, $W = \frac{N^T.N.n_l^2}{M^P - N^T.N.n_l.S}$

$$\left(\frac{\partial f}{\partial \sigma}\right)^T \cdot d\sigma + \left(\frac{\partial f}{\partial \varepsilon_v^p}\right)^T \cdot d\varepsilon_v^p - Y\left(\frac{\partial f}{\partial \sigma}\right)^T \cdot d\sigma - W\left(\frac{\partial f}{\partial s}\right)^T \cdot ds = 0 \rightarrow \lambda = \frac{\left(\frac{\partial f}{\partial \sigma}\right)^T \cdot D^e \cdot d\varepsilon - \frac{W}{1-Y}\left(\frac{\partial f}{\partial s}\right)^T \cdot ds}{\left(\frac{\partial f}{\partial \sigma}\right)^T \cdot D^e \cdot \frac{\partial f}{\partial \sigma} - \frac{1}{1-Y}\left(\frac{\partial f}{\partial \varepsilon_v^p}\right)^T \cdot \frac{\partial f}{\partial \sigma}} \tag{16}$$

Considering the associate flow rule, we have:

$$d\sigma = D^e \cdot d\varepsilon - D^e \cdot \lambda \cdot \left(\frac{\partial f}{\partial \sigma}\right) \rightarrow$$

$$d\sigma = \left[D^e - \frac{D^e.\left(\frac{\partial f}{\partial \sigma}\right) \cdot \left(\frac{\partial f}{\partial \sigma}\right)^T \cdot D^e}{\left(\frac{\partial f}{\partial \sigma}\right)^T \cdot D^e \cdot \frac{\partial f}{\partial \sigma} - \frac{1}{1-Y}\left(\frac{\partial f}{\partial \varepsilon_v^p}\right)^T \cdot \frac{\partial f}{\partial \sigma}}\right] \cdot d\varepsilon - \left[\frac{D^e.\left(\frac{\partial f}{\partial \sigma}\right) \cdot \frac{W}{1-Y}\left(\frac{\partial f}{\partial s}\right)^T}{\left(\frac{\partial f}{\partial \sigma}\right)^T \cdot D^e \cdot \frac{\partial f}{\partial \sigma} - \frac{1}{1-Y}\left(\frac{\partial f}{\partial \varepsilon_v^p}\right)^T \cdot \frac{\partial f}{\partial \sigma}}\right] \cdot ds \tag{17}$$

As shown in the above equation, the elastic matrix is replaced by the two matrixes after considering the elastoplastic model in solid phase simulation by FEM. More information are available in [29].

4. The AMR method for simulating the solid phase in IM3GM

As described in the previous section, the elastoplastic model is added to the solid phase equations, in order to increase the accuracy of determining the deformation. In these conditions, the convergence was not achieved in some areas where deformation increased due to Inability to obtain the exact amount of solid deformation. Also, distribution of permeability, flow pressure, solid stress and mechanical properties are different in the reservoir zones. So, the AMR

method was used in locations where there are critical stresses, such as around the injector and producer wells, or locations where there is a significant heterogeneity around the of the allowed error depends on the accuracy which is needed for each simulation. An error cracks and hydraulic fractures. The AMR method is started in the coarse meshes where the calculated error is more than the allowed error after each iteration. The determination function is defined as following:

$$\|e\|_{\Delta\gamma} = \sqrt{\int_{\Omega} \left(\Delta\gamma^{*} - \Delta\gamma\right)^{2} d\Omega} \tag{18}$$

where $\|e\|_{\Delta\gamma}$ is the error value of an element and Ω is an element domain. Δγ and Δγ* are obtained as follow:

$$d\gamma = \sqrt{1/3\left(\left(d\varepsilon_1^h - d\varepsilon_2^h\right)^2 + \left(d\varepsilon_2^h - d\varepsilon_3^h\right)^2 + \left(d\varepsilon_3^h - d\varepsilon_1^h\right)^2\right)} \tag{19}$$

$$d\gamma^{*} = \sqrt{1/3\left(\left(d\varepsilon_1^{h-1} - d\varepsilon_2^{h-1}\right)^2 + \left(d\varepsilon_2^{h-1} - d\varepsilon_3^{h-1}\right)^2 + \left(d\varepsilon_3^{h-1} - d\varepsilon_1^{h-1}\right)^2\right)} \tag{20}$$

where ε_1, ε_2 and ε_3 are the main strains in the levels *h* or *h-1*. Special care should be taken at coarse-fine interfaces for maintenance of consistency and convergence of the problem. As shown in Fig. 2, the refinement levels start from level 0 (the coarsest) to level *n* (the finest). The level 0 covers the whole area of a problem. The subsequent AMR levels contains smaller and smaller zones of the area. The refinement ratio between any two AMR levels is fixed. This ratio is two in IM^{3}GM. The resuls of each AMR level is maintained in the grids and are used in the next AMR level. Each grid level must be in an area of previous level. The square elements with eight peripheral nodes forming a serendipity family is implemented for both of coarse and refined cells. For more information, please refer to [29, 37].

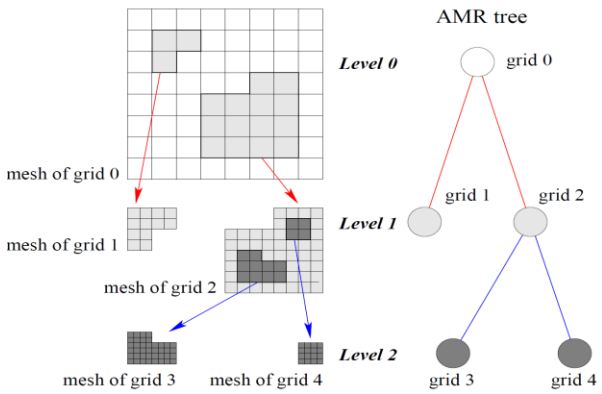

FIG 2. A two dimensional structured AMR instance with quadratic meshes [34].

5. The equations for considering the surrounding rock effects.

It should be noted that the reservoir surrounding environment can effect on solid phase deformations and flow performance. So, the effect of mechanical boundaries around the reservoir is important. However, most of the models which were presented so far have not focused on simulating mechanical boundary conditions. However, some researches increase the accuracy of the presented answers by modeling the reservoir surrounding environment [46-48]. But simultaneous modeling of a reservoir with a wide surrounding area intensively increases computations and modeling costs due to the increase of the number of elements and the number of freedom degrees inside each element. The boundary conditions are corrected based on the resultant pressure and updated until they converge to the desirable limit. The boundary conditions exerted at the sub-zones borderlines are not precise and are exerted in reduced form. In this article, the virtual spring with equivalent rigidity method is used in order to consider the effect of reservoir surrounding rocks. Also, the relevant pattern with corrected boundary conditions is investigated based on the effects of reservoir surrounding rocks on simulation of oil reservoirs. In fact, reservoir supports are not rigid and have a deformation. These displacements can effect on both of reservoir deformation and fluid phase flow. For determining the equivalent rigidity of the reservoir surrounding rocks, unit displacement is exerted on all boundary nodes, separately. The obtained force will be equal to the local rigidity. Reservoir elements and the substituted springs instead of surrounding rocks are shown in Fig. 3. As shown in this figure, the spring stiffness is considered in two orthogonal directions.

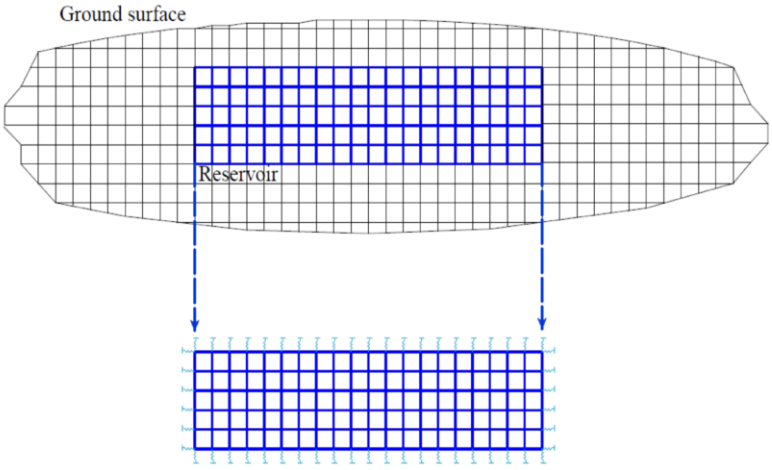

FIG 3. The reservoir elements and substituted springs instead of surrounding rocks in two orthogonal directions

To determine the relevant rigidity, the displacement should be separately exerted in different directions. For instance as shown in Fig. 4, the rigidity of reservoir surrounding rocks at black element is replaced at nodes no 1, 2, 7, 8, 15 and 16. The rigidity of other

nodes of the concerned element will remain as same as before.

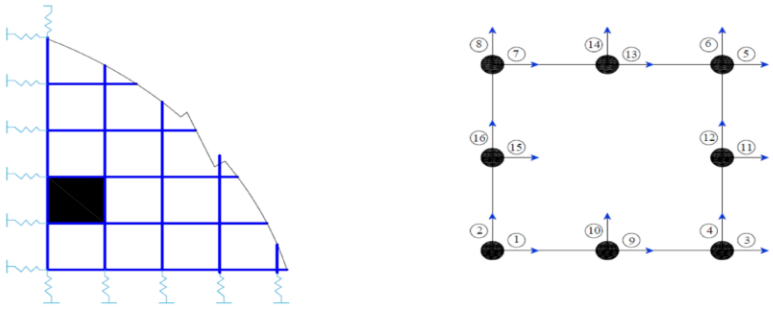

FIG 4. An example for entrance the surrounding rock rigidity on an element

5. Numerical simulation

In IM^{3}GM, the pressure of fluid phases is calculated by conservative MsFV method on fine and coarse networks and the deformation of solid phase is obtained by FEM only on coarse cells, utilizing from AMR method. MsFV consists of three types of coarse network (solid line in Fig. 5-a), dual coarse network (dashed line in Fig. 5-a) and fine network (Fig. 5-b). Coarse network is used to increase the problem scale (reducing computational cost), whereas dual network is used to obtain the unknowns on the micro-scale network, as well as the coarse network. The size of coarse and dual grids is larger than the fine cells which are extracted from the geological model. FEM is performed only on coarse grid. But, if an AMR method is used in a coarse mesh, this mesh in divided to four similar meshes (Fig. 5-c). Almost all MsFV methods use the same viewpoint for making coarse and dual network. On the other hand, quality and method of producing a computational network is a significant element in accuracy, performance and expense of each numerical method. Therefore, the type of computational network can effect on the performance, cost and accuracy of the method. MsFV method consists of four parts and eight steps, which are shown in Fig. 6. The MsFV consists of two main operators. The first one upscales the fine grid geological property with respect to integration fine pressures which are obtained from two sets of shape functions (basis and correction functions). The second operator uses from these two sets to obtain fine-scale pressure and corresponding fine-scale flow over each coarse volume to obtain conservative fine pressure with original resolution. These two functions are the general and particular solutions of Eq. (3) with localized assumptions and reduced boundary conditions on the borders of each dual volume cells. After obtaining the conservative fluid fine pressure, the deformation of solid phase is obtained in adaptive mesh refined coarse cells in terms of fluid pressures. The coupled procedure of Newton iteration loop is applied to consider interactions between fluid pressures and solid deformation. Moreover, physical properties such as degree of saturation and porosity shall be updated in the iterations.

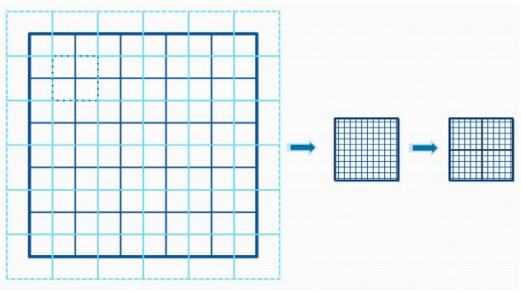

FIG 5. Utilized networks in IM^{3}GM which are a) coarse network (murky line), dual coarse network (bright line), b) fine network in a coarse cell and c) a refined coarse cell and containing fine cells after one-level of AMR

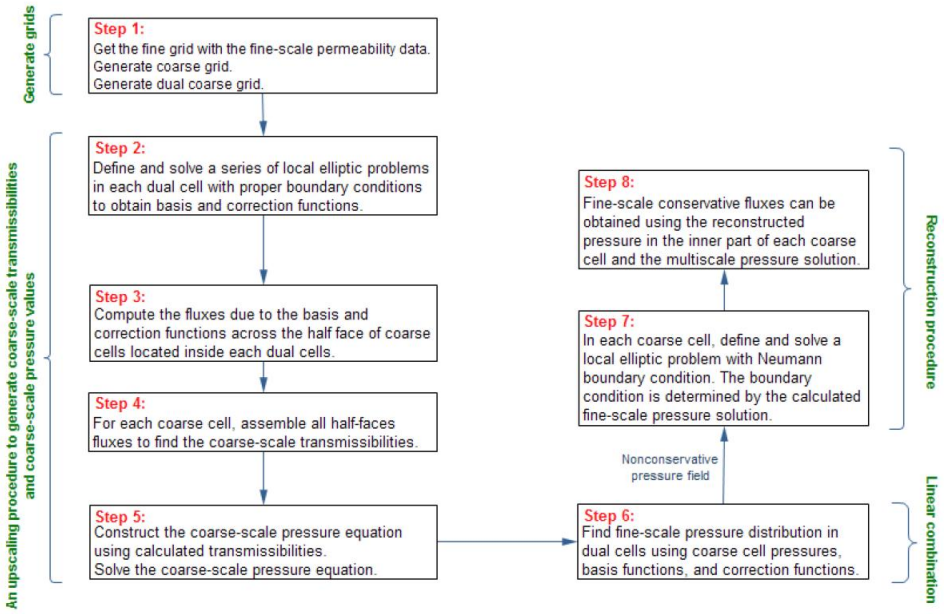

FIG 6. the four parts and eight steps of MsFV method

In simulation by IM^{3}GM, first, the equations of fluid phases are solved in the center of the coarse scale, using dual and coarse mesh networks, and fluid pressures are obtained in coarse scale. Then, fluid pressures are gained in fine scale, utilizing coarse scale results. After fluid pressures converged between coarse and fine scales, it is used to obtain deformations in solid phase on coarse scale, using an AMR method and considering surrounding effects. Deformation is used to obtain fluid pressures in the next level of the analysis. This cycle is repeated again and again. The obtained pressures in different cells are non-conservative. So, the pressure equations are solved again on the boundaries of coarse cells by Newman boundary conditions, in order the degree of saturation to be updated according to conservative pressures. Basis and correction functions are the general and particular solutions of Eq. (5), after localization of boundaries. Next, the deformation of solid phase is obtained by FEM on coarse cells in terms of fluid

pressures considering the AMR method. The second term on the right-hand side of the eq. (21) which is writhed based on FEM, is obtained by integrating over all fine cells encapsulated in each coarse or refined coarse cells. The coupled Newton iteration loop is used to consider the interactions between fluid pressures and solid strains. Also, porosity and saturation degree are updated in each iteration. For more information about basic and correction functions and how to update these functions please refer to [15, 16].

$$\left[\int_{\Omega}\mathbf{B}^{T}\mathbf{D}\mathbf{B}\;\;d\Omega\right].\hat{\mathbf{u}}=-\int_{\Gamma^{N}}\mathbf{N}_{u}^{T}\bar{t}d\Gamma+\int_{\Omega}\mathbf{B}^{T}(p\mathbf{m})d\Omega \qquad (21)$$

For completely solving the equation, first the main equation is divided to two sections: general section (without right hands side) and particular section (with right hand side). Then, the mentioned shape functions are exerted to the zone, which have been exerted on boundary conditions in form of Dirichlet conditions. However, it should be noted that computation cost of basic functions is four times more than corrective functions. Therefore, after exerting boundary conditions on each sub-zones, separation occurs and all the pressure-related values (fluid phase density and solid phase deformation) to be performed by corrective functions. Also, basic functions are updated based on the variation in mobility ratio which is related to the saturation degree. Solving transfer equation occurs explicitly at each time step for determining the saturation degree of each phase. So, the computing basic functions which constitute the main part of computations gets out of the pressure cycle. Moreover, as it will be explained in the following, reservoir analysis only effects on a small part of saturation degree in each iteration. Therefore, updating basic functions will be only performed for subsidiary elements to increase the computational efficiency. Also, it is hardly required to solve pressure equation in each time step, because permeability changes during times is calm in comparison to permeability changes due to situation variations. Therefore, in many points of solution area, properties are very similar to the properties of those areas in the previous time step, and there is no need for updating.

6. Numerical Results

As previously mentioned, the surrounding environment of a reservoir can effect on its performance. To study the quality and value of this effect, a complex heterogeneous deformable porous media of the top layer of the SPE10 is modeled and compared by considering the effect of the surrounding environment. Also, at the right and left side of the reservoir, an environment ten times more than the reservoir length is taken into account to consider its effect on the reservoir deformation. The height of rock layers are selected to be 100 meters at the top of the reservoir.

As mentioned in last section, the stiffness of equivalent springs is the result of applying the unit force and dividing it to the resulted deformation in each node. As the simulated case, transformable heterogeneous medium with surrounding rock layers is taken into account, and permeability is extracted from the top layer of SPE 10. The permeability

natural logarithm and fluid characteristics in fine scale are shown in Fig. 7. The geomechanical properties of the reservoir in large scale is shown in Fig. 8. Porous medium has 60×40 fine elements and 12×8 coarse cells in the start on an analysis. Injection takes place from fine cell (1,1) with a five times less viscous fluid and production occurs from cell (37,52) with a constant rate pressure of 10kPa. No-flow boundary conditions apply at the domain borders. The elasticity modulus of the surrounding rock is considered to be 5GPa or 10GPa to assess the reservoir surrounding environment. Reservoir environment includes 80 percent of oil and 20 percent of water. The production rate in different analysis cases are shown in Fig. 9.

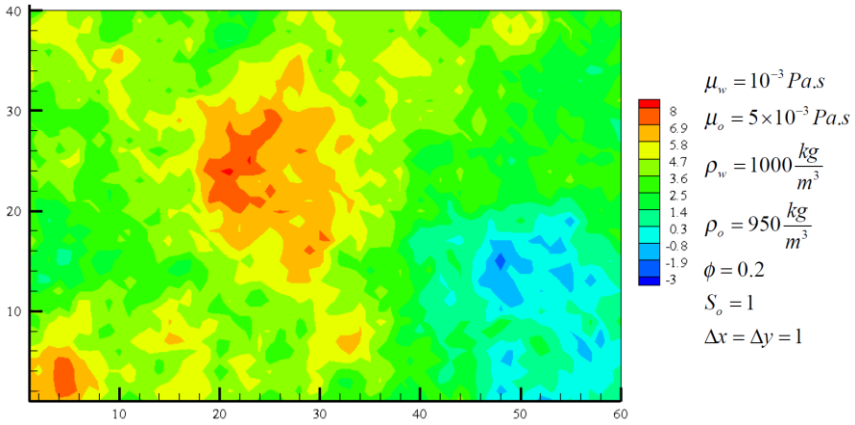

FIG 7. Natural logarithm of the permeability and physical fluid properties of the investigated case

As shown in Fig. 9, production rate in a rigid condition is more than considering reservoir deformation especially in the beginning of production. It is due to disregarding a part of injection energy which is exhausted by the deformation of porous medium. This process will continue until injection finishes. Because even if the stress is constant, still a part of energy will be used to deformation of the porous medium, and hence will be exhausted. Also as seen in Fig. 9, the reservoir surrounding environment has also an important effect on the production rate. Similarly, how the reservoir surrounding environment is more rigid and has the rocks with higher elasticity modulus, the energy exhaustion is reduced and production rate is increased. Also, in the case of deformable porous medium, pressure is lower than the rigid case. In fact, considering the porous medium deformation, injection pressure is not completely imported to the fluid, and a part of it causes solid phase deformation.

As shown in Fig. 9, in elastoplastic mode, it takes longer for production rated to reach to constant rate. As shown in this figure, the stability value of production rate increases in more rigid surrounding environment which is in compliance with the results obtained by other refrences [49, 50]. Also deformation contours are shown in Fig. 10 for elastoplastic mode. The maximum deformation is observed at the top of the injection well. Therefore, it should be kept in mind that sensitive equipment such as emergency shutdown valves, launcher trap, saving tanks with floating roof should not be located in this place, or necessary

arrangements should be taken to control them.

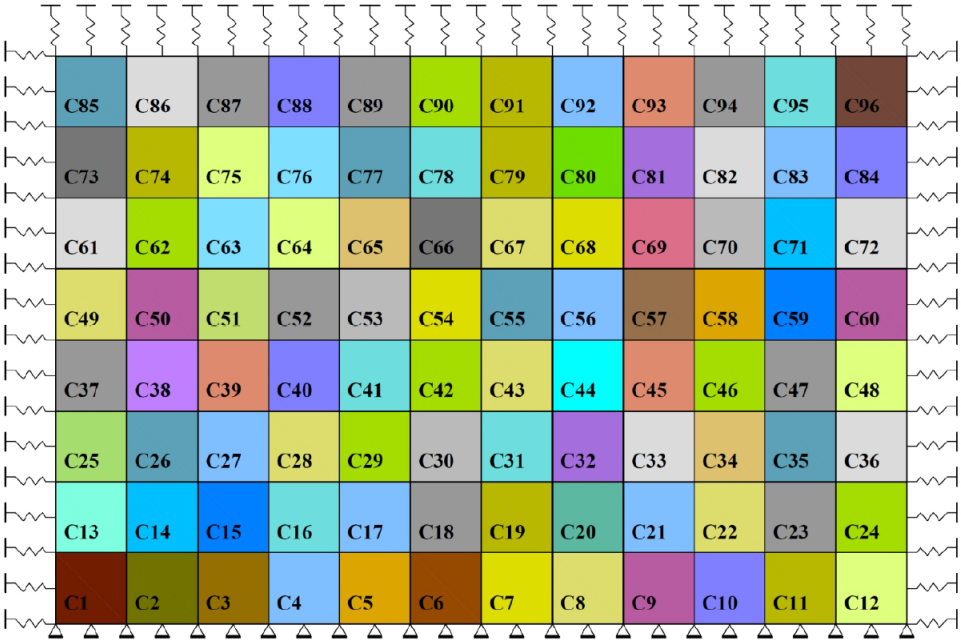

Log. No:	E_{ini}	υ	χ	n	Log. No:	E_{ini}	υ	χ	n	Log. No:	E_{ini}	υ	χ	n	Log. No:	E_{ini}	υ	χ	n
C1	8.0E+09	0.21	1.05	0.03	C25	4.4E+07	0.31	1.2	0.03	C49	2.8E+07	0.22	1.2	0.03	C73	2.8E+07	0.22	1.2	0.01
C2	1.6E+09	0.22	1.05	0.02	C26	2.4E+07	0.21	1.25	0.02	C50	3.6E+07	0.24	1.1	0.01	C74	3.6E+07	0.22	1.15	0.02
C3	1.2E+09	0.23	1.07	0.02	C27	6.8E+07	0.18	1.03	0.01	C51	4.8E+07	0.24	1.3	0.02	C75	4.8E+07	0.21	1.15	0.03
C4	8.0E+08	0.24	0.08	0.03	C28	7.2E+07	0.16	1.02	0.03	C52	5.6E+07	0.25	1.25	0.01	C76	5.6E+07	0.24	1.2	0.02
C5	4.0E+08	0.21	1.1	0.01	C29	8.8E+07	0.22	1.02	0.02	C53	6.0E+07	0.25	1.1	0.03	C77	6.0E+07	0.24	1.15	0.01
C6	3.2E+08	0.2	1.2	0.01	C30	8.4E+07	0.21	1.2	0.02	C54	5.4E+07	0.25	1.1	0.02	C78	5.4E+07	0.24	1.2	0.02
C7	2.4E+08	0.25	1.3	0.01	C31	1.3E+08	0.16	1.2	0.02	C55	5.8E+07	0.25	1.1	0.02	C79	5.8E+07	0.22	1.25	0.01
C8	3.2E+08	0.21	1.01	0.01	C32	1.1E+08	0.14	1.12	0.02	C56	5.1E+07	0.18	1.3	0.02	C80	5.1E+07	0.22	1.2	0.02
C9	4.8E+08	0.22	1.1	0.02	C33	8.4E+07	0.25	1.14	0.01	C57	5.0E+07	0.22	1.15	0.02	C81	5.0E+07	0.22	1.1	0.01
C10	3.6E+08	0.23	1.2	0.01	C34	8.0E+07	0.26	1.16	0.02	C58	4.4E+07	0.32	1.2	0.02	C82	4.4E+07	0.22	1.05	0.01
C11	4.4E+08	0.21	1.25	0.01	C35	7.2E+07	0.27	1.2	0.01	C59	4.8E+07	0.32	1.2	0.02	C83	4.8E+07	0.3	1.1	0.01
C12	4.0E+08	0.22	1.1	0.01	C36	8.0E+07	0.28	1.12	0.03	C60	4.8E+07	0.25	1.2	0.03	C84	5.6E+07	0.3	1.1	0.01
C13	4.0E+07	0.26	1.08	0.01	C37	3.2E+07	0.32	1.16	0.02	C61	3.4E+07	0.25	1.15	0.01	C85	2.8E+07	0.22	1.1	0.02
C14	4.8E+07	0.27	1.1	0.02	C38	3.6E+07	0.18	1.06	0.01	C62	3.6E+07	0.25	1.25	0.02	C86	3.6E+07	0.22	1.08	0.01
C15	5.6E+07	0.28	1.09	0.02	C39	4.8E+07	0.22	1.08	0.01	C63	4.8E+07	0.3	1.25	0.02	C87	4.8E+07	0.25	1.08	0.03
C16	4.8E+07	0.23	1.05	0.02	C40	5.6E+07	0.18	1.12	0.02	C64	5.6E+07	0.28	1.1	0.01	C88	5.6E+07	0.28	1.08	0.02
C17	4.4E+07	0.24	1.2	0.02	C41	6.0E+07	0.25	1.3	0.02	C65	6.0E+07	0.28	1.1	0.02	C89	6.0E+07	0.24	1.2	0.02
C18	5.6E+07	0.25	1.02	0.02	C42	7.2E+07	0.25	1.5	0.01	C66	5.4E+07	0.25	1.1	0.01	C90	5.4E+07	0.22	1.1	0.03
C19	3.6E+07	0.2	1.2	0.02	C43	5.8E+07	0.25	1.6	0.03	C67	5.8E+07	0.25	1.2	0.03	C91	5.8E+07	0.25	1.09	0.01
C20	4.0E+07	0.3	1.02	0.03	C44	5.1E+07	0.25	1.8	0.01	C68	5.1E+07	0.25	1.2	0.02	C92	5.1E+07	0.25	1.1	0.02
C21	4.8E+07	0.22	1.3	0.01	C45	5.0E+07	0.22	2	0.02	C69	5.0E+07	0.25	1.2	0.02	C93	5.0E+07	0.24	1.1	0.01
C22	4.4E+07	0.15	1.4	0.02	C46	4.4E+07	0.24	1.8	0.02	C70	4.4E+07	0.25	1.4	0.02	C94	4.4E+07	0.22	1.08	0.03
C23	5.2E+07	0.18	1.05	0.01	C47	4.8E+07	0.28	1.2	0.02	C71	4.8E+07	0.28	1.1	0.01	C95	4.8E+07	0.26	1.15	0.02
C24	6.0E+07	0.32	1.02	0.01	C48	5.0E+07	0.2	1.2	0.01	C72	4.8E+07	0.28	1.1	0.01	C96	4.8E+09	0.24	1.2	0.01

FIG 8. Geomechanical specifications and boundary springs of an investigated oil reservoir

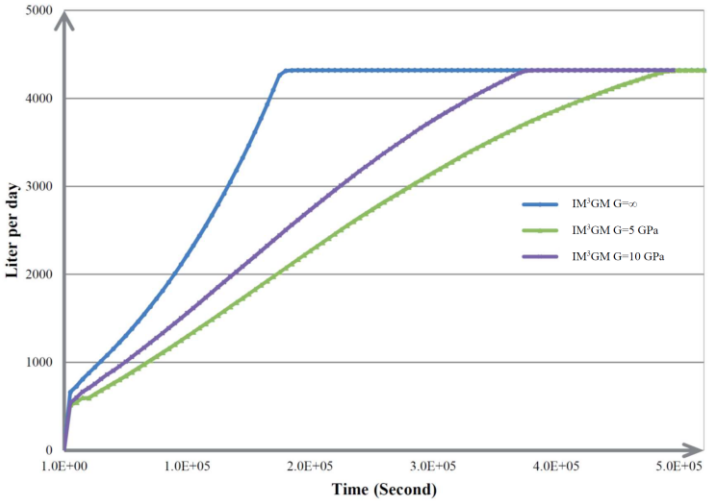

FIG 9. Comparing the production rate of simulated oil reservoir with different surrounding elasticity modulus

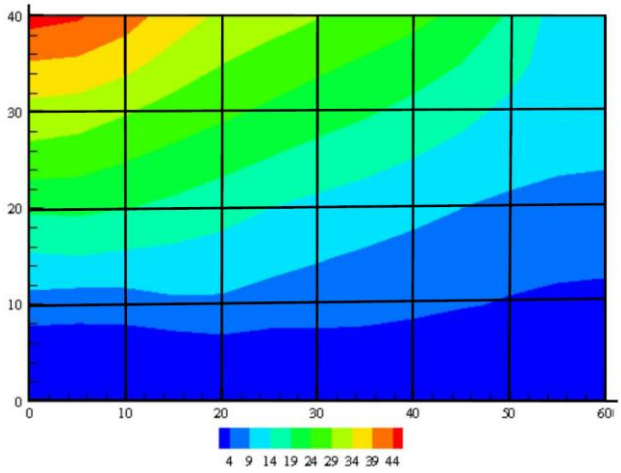

FIG 10. Deformation distribution of simulated oil reservoir which simulated by IM³GM after 0.085 pore volume injection

7. Conclusion

Management of oil reservoirs and the development of new fields require reservoir simulations. The Improved Multiscale Multiphysic Mixed Geomechanical Model (IM³GM) is presented as a way to deal with the multiscale nature of reservoir rocks taking into consideration any physical phenomenon in its region of influence, specially surrounding rocks. Also, the capillary pressures were added in the equations of fluid phases. Moreover, this model considers an elastoplastic behavior of porous media in solid phase using an AMR method. Finally, the effect of surrounding rock were considered in this model. It demonstrates that neglecting the deformation of reservoir solid phase and also neglecting the deformation of surrounding rock, leads to overestimation of production rates and mislead optimization

strategies.

8. Acknowledgement

The author expresses sincere thanks to Mohammad Sanayepasand for performing the numerical simulation.

9. References

[1] Lunati, I.; Jenny, P; (2006); "Multiscale finite-volume method for compressible multiphase flow in porous media", Computational Pysics, 216, 616-636.

[2] Hou, T. Y.; Wu, X. H.; (1997); "A multiscale finite element method for elliptic problems in composite materials and porous media", Computational Pysics, 134, no. 1, 169–189.

[3] Dehkordi, M. M.; Manzari, M. T.; (2013); "Effects of using altered coarse grids on the implementation and computational cost of the multiscale finite volume method", Adv. Water Resour., vol. **59**, 221–237.

[4] Jenny, P.; Lee, S., H.; Tchelepi, H., A.; (2003); "Multi-scale finite-volume method for elliptic problems in subsurface flow simulation", Coputational Physics, 187, 47-67.

[5] Jenny, P.; Lee, S., H.; Tchelepi, H., A.; (2004); "Adaptive Multiscale Finite-Volume Method For Multiphase Flow And Transport In Porous Media. Multiscale Model", Simul., 3, 50–64.

[6] Tchelepi, H. A.; Jenny, P.; Lee, S. H.; Wolfsteiner, C.; (2005); "An adaptive multiphase multiscale finite volume simulator for heterogeneous reservoirs," in SPE Reservoir Simulation Symposium.

[7] Jenny, P.; Lee, S., H.; Tchelepi, H, A.; (2006); "Adaptive fully implicit multi-scale finite-volume method for multi-phase flow and transport in heterogeneous porous media", Journal of Computational Physics, 217(2), 627-641.

[8] Lunati, I.; Jenny, P.; (2008); "Multiscale finite-volume method for density-driven flow in porous media," *Comput Geosci*, vol. 12, no. 3, 337–350.

[9] Lunati, I.; Jenny, P.; (2006); "A multiscale finite-volume method for three-phase flow influenced by gravity," XVI International Conference on Computational Methods in Water Resources (CMWR XVI), Copenhagen, *Denmark*, pp. 1–8.

[10] Zhou, H.; Tchelepi, H.; (2008); "Operator-based multiscale method for compressible flow", SPE J., vol. 13, no. 2, 267–273.

[11] Lunati, I.; Lee, S. H.; (2009); "An operator formulation of the multiscale finite volume method with correction function", *Multiscale Model and Simul*, vol. 8, 96–99.

[12] Hajibeygi, H., Bonfigli, G., Hesse, M. A., Jenny, P., (2008); "Iterative multiscale finite-volume method", Computational Physic, 227, 8604–8621.

[13] Hajibeygi, H.; Jenny, P.; (2009); "Multiscale finite-volume method for parabolic problems arising from compressible multiphase flow in porous media", Computational Physics, 228, 5129-5147.

[14] Wang, Y.; Hajibeygi, H.; Tchelepi, H.; (2012); "Algebraic multiscale linear solver for heterogeneous elliptic problems", 13th European Conference of Mathematics of Oil Recovery (ECMOR XIII), Biarritz, France, 1–7.

[15] Sadrnejad, S. A.; Ghasemzadeh, H.; Taheri, E.; (2014); "Multiscale multiphysic mixed geomechanical model in deformable porous media", *J. Multiscale Comput. Eng*., vol. **12**, no. 6, 529–547.

[16] Taheri, E.; Sadrnezhad, S., A.; Ghasemzadeh, H.; (2015); "Multiscale geomechanical model for a deformable oil reservoir with surrounding rock effects", International journal for multiscale computational engineering, 13 (6), 533-559.

[17] Tomin, P.; Lunati, I.; (2015); "Local–global splitting for spatiotemporal-adaptive multiscale methods", Journal of Computational Physics, 280, 214-231.

[18] Fouladi Moghaddam, N., Mexico, s. n.; (2010); "*Subsidence monitoring of an Iranian oil field inferred from SAR interferometry",* Land Subsidence, Associated Hazards and the Role of Natural Resources Development. pp. 299- 303.

[19] Wheeler, S.; Sharma, R.; Buisson, M.; (2003); "Coupling of hydraulic hysteresis and stress– strain behavior in unsaturated soils", Geotechnique, vol. 53(1), 41–53.

[20] Sun, D.; Sheng, D.; Sloan, S.; (2007); "Elastoplastic modelling of hydraulic and stress–strain behaviour of unsaturated soils", Mech Mater, vol. 39, 212–21.

[21] Thu, T. M.; Rahardjo, H.; Leong, E. C.; (2007); "Elastoplastic model for unsaturated soil with incorporation of the soil-water characteristic curve", Can Geotech J, vol. 44(1), 67-77.

[22] Muraleetharan, K.; Liu, C.; Wei, C.; Kibbey, T.; Chen, L.; (2009); "An elastoplastic framework for coupling hydraulic and mechanical behavior of unsaturated soils", Int J Plast, vol. 25(3), 473–90.

[23] Ghasemzadeh, H.; (2008); "Heat and contaminant transport in unsaturated soil", Int. J. Civ. Eng., Vol. 6, 90-107.

[24] Masın, D.; (2010);"Predicting the dependency of a degree of saturation on void ratio and suction using effective stress principle for unsaturated soils", Int J Numer Anal Methods Geomech, vol. 34, 73–90.

[25] D'Onza, F.; Gallipoli, D.; Wheeler, S.; Casini, F.; Vaunat, J.; Khalili, N.; (2010); "Benchmarking different approaches to constitutive modelling of unsaturated soils", Geotechnique, vol. 61(4), 283–302.

[26] Sun, D.; Sun, W.; Xiang, L. .; (2010); "Effect of degree of saturation on mechanical behavior of unsaturated soils and its elastoplastic simulation", Comput Geotech, vol. 37(5), 678–88.

[27] Ghasemzadeh, H.; Ghoreishian Amiri, S. A.; (2013); "A hydro-mechanical elastoplastic model for unsaturated soils under isotropic loading conditions", Comput Geotech, vol. 51, 91-100.

[28] Ghasemzadeh, H.; Sojoudi, M. H.; Ghoreishian Amiri S. A.; Karami M. H.; (2017); "An elastoplastic model for hydro-mechanical behavior of unsaturated soils, Soils and Foundations", vol. 57 (3), 371-383.

[29] Ghasemzadeh, H.; Sanaye Pasand, M.; (2019); "An elastoplastic model for oil reservoirs using multiscale and adaptive mesh refinement methods", International journal for multiscale computational engineering, submitted.

[30] Chen, X.; Yang, V.; (2014); "Thickness-based adaptive mesh refinement methods for multi-phase flow simulations with thin regions", Coputational Physics, vol. 269, 22-39.

[31] Popinet, S.; (2009); "An accurate adaptive solver for surface–tension–driven interfacial flows", J. Comput. Phys., vol. 228, 5838–5866.

[32] Xie, Z.; Pavlidis, D.; Percival, J. R.; Gomes, J. L. M. A.; Pain, C. C.; Matar, O. K.; (2014); "Adaptive unstructured mesh modelling of multiphase flows", Multiphase Flow, vol. 67, 104-110.

[33] Lovett, S.; Nikiforakis, N.; Monmont, F.; (2015); "Adaptive mesh refinement for compressible thermal flow in porous media", Coputational Physics, vol. 280, 21-36.

[34] Liao, W. K.; Liu, Y.; Choudhary, A.; (2002); "A Grid-based Clustering Algorithm using Adaptive Mesh Refinement".

[35] Brown, J. D.; Lowe, L. L.; (2005); "Multigrid elliptic equation solver with adaptive mesh refinement", J. Comput. Phys. (ISSN0021-9991), vol. 209(2), 582–598.

[36] Khoei, A. R.; Gharehbaghi, S. A.; Tabarraie, A. R.; Riahi, A.; (2007); "Error estimation, adaptivity and data transfer in enriched plasticity continua to analysis of shear band localization", Applied Mathematical Modelling ,vol. 31, 983–1000.

[37]Ghasemzadeh, H.; Sanaye Pasand, M.; (2018); "Modeling of oil transport in porous media using multiscale method with adaptive mesh refinement, Energy Geotechniques", 475-485.

[38] Rothenburg, L., Bratli, R.K. and Dusseault, M.B.; (1994); "A poro- elastic solution for transient fluid

flow into a well", Canda : PMRI Publications, University of Waterloo.

[39] Subsidence monitoring of an Iranian oil field inferred from SAR interferometry. Fouladi Moghaddam, N., et al. Mexico, s.n.; (2010); "Associated Hazards and the Role of Natural Resources Development", Land Subsidence, 299- 303.

[40] Yin, s.; (2008); "Geomechanics- Reservoir Modeling by Displacement Discontinuity- Finite Element Method", PhD Dissertation, University of Waterloo.

[41] Settari, A; (2002); "Reservoir compaction", Journal of Petroleum Technology, Vol. 54, 62- 69.

[42] Wang, W.; (2012); "Numerical study of mixing behavior with chemical reactions in micro- channels by a lattice Boltzmann method", Chemical Engineering Science, Vol. 84, 148–154.

[43] Hou, Q. F.; Zhou, Z. Y; Yu, A. B; (2012); "Micromechanical modeling and analysis of different flow regimes in gas fluidization", Chemical Engineering Science, Vol. 84, 449–468.

[44] Farajzadeha, R.; (2012); "Foam–oil interaction in porous media: Implications for foam assisted enhanced oil recovery", Advances in Colloid and Interface Science, Vols. 183- 184, 1–13.

[45] Kim, Y.; Jeong, S.; Kim, J.; (2016); "Coupled infiltration model of unsaturated porous media for steady rainfall", Soils and Foundations, vol. 56(6), 1071–1081.

[46] Rothenburg, L.; Bratli, R. K; Dusseault, M. B.; (1994); "A Poroelastic Solution for Transient Fluid Flow into a Well", University of Waterloo, Canada, PMRI Publications.

[47] Yin, Sh.; Rothenburg, L.; Dusseault, M. B.; (2006); "3D Coupled Displacement Discontinuity and Finite Element Analysis of Reservoir Behavior during Production in Semi-infinite Domain. Transport in Porous Media", 65, 425-441.

[48] Yin, Sh.; Dusseault, M. B.; Rothenburg, L.; (2007); "Coupled multiphase poroelastic analysis of reservoir depletion including", International Journal of Rock Mechanics & Mining Sciences, 44, 758–766.

[49] Sone, H.; (2012) "Mechanical properties of shale gas reservoir rocks and its relation to the in-situ stress variation observed in shale gas reservoirs". PHD thesis, Standford university.

[50] Sone, H.; Zoback, M. D.; (2014); "Time-dependent deformation of shale gas reservoir rocks and its long-term effect on the in situ state of stress", International Journal of Rock Mechanics & Mining Sciences, 69, 120–132.